Theoretical and Applied Fracture Mechanics 100 (2019) 78–85

Contents lists available at ScienceDirect

Theoretical and Applied Fracture Mechanics

journal homepage: www.elsevier.com/locate/tafmec

A generalized maximum energy release rate criterion for mixed mode fracture analysis of brittle and quasi-brittle materials

Cheng Hou[a], Xiaochao Jin[a], Xueling Fan[a,*], Rong Xu[b,*], Zhiyong Wang[c]

[a] State Key Laboratory for Strength and Vibration of Mechanical Structures, School of Aerospace Engineering, Xi'an Jiaotong University, Xi'an 710049, China
[b] School of Mechanical Engineering, Purdue University, West Lafayette, IN 47907, USA
[c] Institute of Applied Mechanics, College of Mechanical and Vehicle Engineering, Taiyuan University of Technology, Taiyuan 030024, China

ARTICLE INFO

Keywords:
Maximum energy release rate criterion
Mixed mode fracture
T-stress
Fracture initiation angle
Fracture resistance

ABSTRACT

A modified mixed mode fracture criterion, called generalized maximum energy release rate criterion, is proposed to predict the fracture initiation angles and estimate the fracture resistances in brittle and quasi-brittle materials under mixed mode loading. With this generalized maximum energy release rate criterion, the energy release rate around the crack tip is calculated by considering the contributions from both singular stress terms and T-stress. Experimental data, extracted from prior literatures for central cracked Brazilian disk, cracked semi-circular bend and edge-crack triangular specimens, are used to validate the modified criterion and evaluate the accuracy of the prediction obtained from this modified criterion. Results show that the T-stress plays a remarkable role in the mixed mode I/II fracture analysis when the energy-based criterion is employed. In addition, it is shown that the modified criterion can well predict the mixed mode I/II fracture behaviors of brittle and quasi-brittle materials.

1. Introduction

Mechanical reliability is a critical issue in many engineering applications such as aerospace craft and nuclear power station. During their service, fracture of materials or structures is difficult to avoid and often constitutes the major mechanical failure [1–3]. Therefore, a good understanding on the fracture behaviors of materials or structures is important and necessary. Many efforts have been made before to establish failure criteria and determine the fracture toughness for different materials [4–6]. In the past few decades, a series of fracture criteria have been proposed and widely used to predict the initiation and propagation of cracks [7–23], as summarized in Table 1. These criteria can be divided into three categories: stress-based criteria [7–9], strain-based criteria [10–13] and energy-based criteria [14–23]. There are three classical fracture criteria in fracture mechanics, i.e. the maximum tangential stress (MTS) criterion [7], minimum strain energy density (SED) criterion [14] and maximum energy release rate (G) criterion [19–21]. The MTS criterion is a stress-based criterion, and the SED and G criteria are the energy-based criteria. These criteria have been widely applied to study brittle fracture in various materials such as ceramics, rocks, glasses, brittle polymers and polymeric foam materials.

However, these criteria could not able to accurately predict the onset of mixed mode fracture (combination of the mode I, mode II or mode III cracks), mainly owing to the significant difference between the theoretical prediction and experimental results [24–28]. This difference is probably attributed to the fact that all these criteria only include the influence of singular stress terms in Williams' series expansion (i.e. stress intensity factors, SIFs) but ignore the higher order terms of the expansion. Although the singular stress terms in Williams' series expansion can roughly represent the driving force for crack growth, the neglection of higher order stress terms might deviate the calculated stress fields from the accurate one around the crack tip [15,18]. In this scenario, fracture behaviors predicted by the classical criteria might not agree well with the experimental results, especially for mode II dominant fracture behaviors [11–13,15,18].

To better predict the initiation and propagation of mixed mode cracks in brittle and quasi-brittle materials, researchers developed the modified fracture criteria by including both the singular and non-singular stress terms in Williams' series expansion [8,9,11–13,15,18]. The first non-singular stress term in Williams' series expansion, called T-stress, acts parallel to the crack line with a magnitude proportional to the gross stress in the vicinity of the crack, and is proved to have a significant influence on both the fracture initiation angles and the onset of fracture [8,29]. A generalized maximum tangential stress (GMTS) criterion was proposed by Smith et al. [8] to evaluate the effect of T-stress on the brittle fracture under mixed mode loading conditions. Later, a series of experiments [24,30–34] confirmed that fracture behaviors of brittle or quasi-brittle materials under mixed mode loading

* Corresponding authors.
E-mail addresses: fanxueling@mail.xjtu.edu.cn (X. Fan), xu666@purdue.edu (R. Xu).

https://doi.org/10.1016/j.tafmec.2018.12.015
Received 12 December 2018; Received in revised form 28 December 2018; Accepted 28 December 2018
Available online 30 December 2018
0167-8442/

Table 1
A list of three criteria categories: stress-based criteria, strain-based criteria and energy-based criteria.

	Criteria	References
Stress-based	Maximum tangential stress criterion, MTS	Erdogan and Sih [7]
	Generalized maximum tangential stress criterion, GMTS	Smith et al. [8]
	Modified maximum tangential stress criterion, MMTS	Akbardoost and Ayatollahi [9]
Strain-based	Maximum tangential strain criterion, MTSN	Chang [10]
	Extended maximum tangential strain criterion, EMTSN	Mirsayar et al. [11,12] and Hua et al. [13]
Energy-based	Strain energy density criterion, SED	Sih [14]
	Generalized strain energy density criterion, GSED	Ayatollahi et al. [15]
	Averaged strain energy density criterion, ASED	Lazzarin and Zambardi [16]
	Generalized averaged strain energy density criterion, GASED	Moghaddam et al. [18]
	Maximum energy release rate criterion, G	Palaniswamy [19], Hussain et al. [20] and Nuismer [21]

agreed well with the prediction by the GMTS criterion. Another fracture criterion, modified maximum tangential stress (MMTS) criterion [9], was developed by including both singular stress terms (SIFs) and three non-singular stress terms (i.e. T-stress, A_3 and B_3, where A_3 and B_3 are the second non-singular stress terms in Williams' series expansion) into consideration and employed to estimate the mixed mode fracture resistances of Neyriz marble samples. In additional to stress-based criteria, a few strain-based criteria have been also modified by including the effects from the T-stress, such as the extended maximum tangential strain (EMTSN) criterion [11–13]. Similarly, energy-based criteria have also been modified to evaluate the mixed mode fracture. Ayatollahi et al. [15] improved the SED criterion into a generalized strain energy density (GSED) criterion for mixed mode fracture analysis of brittle and quasi-brittle materials, by including three key factors, mode I SIF (K_I), mode II SIF (K_{II}) and T-stress. Later, Moghaddam et al. [18] proposed a generalized averaged strain energy density (GASED) criterion to predict mixed mode I/II fracture behaviors of brittle and quasi-brittle materials. It also accounted the effect of T-stress on the calculation of the averaged strain energy density around the crack tip. In summary, no matter relying on stress-based, strain-based or energy-based fracture criteria, results indicated that T-stress had a remarkable influence on the mixed mode fracture behaviors of brittle and quasi-brittle materials, including both fracture initiation angles and fracture resistances.

Maximum energy release rate criterion (also called G criterion), one of the classical mixed mode crack criteria, has been extensively utilized to predict the initiation of mixed mode cracks through calculating the energy release rate around the crack tip [20–23]. However, similar with previous classic criteria, conventional G criterion only includes the singular stress terms in Williams' series expansion with ignoring the influence of non-singular stress terms when describing the stress fields in the vicinity of crack tip, resulting in some divergences between the theoretical results and experimental results, especially when mode II fracture are predominant. To our best knowledge, no available G criterion that includes the influence from the non-singular stress terms is established to accurately predict the mixed mode I/II fracture behaviors. Therefore, in this paper, a generalized form of G criterion is proposed to study the mixed mode I/II fracture behaviors for brittle and quasi-brittle materials. This proposed criterion considers the influence from not only singular stress terms (SIFs) but also the first non-singular stress term (T-stress) in Williams' series expansion on the calculation of energy release rate of crack growth. The experimental results, reported in prior literatures [26,27,34] on the fracture analysis of central cracked Brazilian disc (CCBD), cracked semi-circular bend (SCB) and edge-crack triangular (ECT) specimens, are used to verify the accuracy of the proposed generalized G criterion.

2. Generalized maximum energy release rate criterion

The generalized G criterion is derived to study the mixed mode I/II fracture behaviors in this section. For a plane crack problem, as shown in Fig. 1, Williams [35] proposed a set of infinite series expansions to

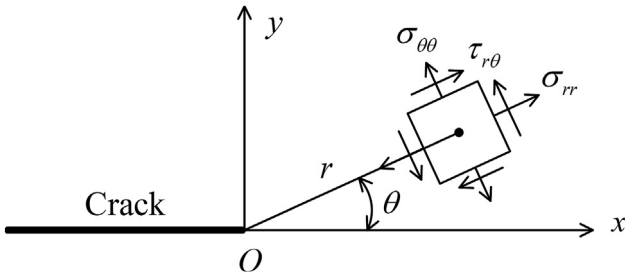

Fig. 1. Stress components in the polar coordinate around the crack tip.

describe the elastic stress fields around the crack tip, as follows:

$$\sigma_{\theta\theta} = \frac{1}{2\sqrt{r}}\left[\frac{K_I}{\sqrt{2\pi}}(1+\cos\theta)\cos\frac{\theta}{2} - 3\frac{K_{II}}{\sqrt{2\pi}}\sin\theta\cos\frac{\theta}{2}\right] + T\sin^2\theta + O(r^{1/2}) \quad (1)$$

$$\sigma_{rr} = \frac{1}{2\sqrt{r}}\left[\frac{K_I}{\sqrt{2\pi}}(3-\cos\theta)\cos\frac{\theta}{2} + \frac{K_{II}}{\sqrt{2\pi}}(3\cos\theta-1)\sin\frac{\theta}{2}\right] + T\cos^2\theta + O(r^{1/2}) \quad (2)$$

$$\tau_{r\theta} = \frac{1}{2\sqrt{r}}\left[\frac{K_I}{\sqrt{2\pi}}\sin\theta + \frac{K_{II}}{\sqrt{2\pi}}(3\cos\theta-1)\right]\cos\frac{\theta}{2} - T\sin\theta\cos\theta + O(r^{1/2}) \quad (3)$$

where $\sigma_{\theta\theta}$, σ_{rr} and $\tau_{r\theta}$ are elastic stresses in the polar coordinate system and (r, θ) are the crack tip coordinates (see Fig. 1). K_I and K_{II} are the SIFs of the mode I and mode II fracture, respectively. T is the first non-singular stress term, which is called T-stress. The higher order non-singular stress terms $O(r^{1/2})$ are usually negligible near the crack tip [26,27,34].

When the stress intensity at pre-existing crack tip increases to a certain level, the crack will extend a small length $\bar{a}$ to form a branch crack, not necessarily along the direction of the original crack, but along an arbitrary direction θ_0, as shown in Fig. 2. Once a branch crack forms, the calculation of energy release rate for the branch crack

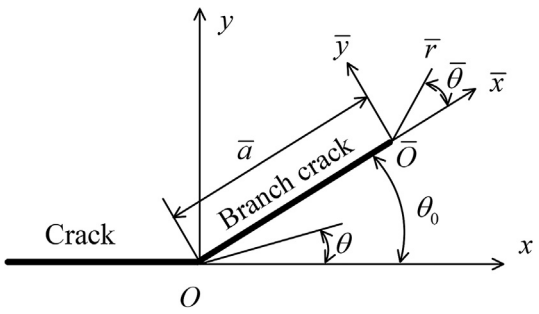

Fig. 2. Geometry and coordinate systems for the branch crack.

becomes challenging due to the complicated boundary value problems [21]. If we only focus on the initiation of fracture, instead of fracture propagation, the length of branch crack $\bar{a}$ can be assumed to shrink to zero. It indicates that the stresses (such as $\bar{\sigma}_{\bar{y}}$ and $\bar{\tau}_{\bar{x}\bar{y}}$) around the tip of branch crack are approximately equal to the stresses (such as $\sigma_{\theta\theta}$ and $\tau_{r\theta}$) at the tip of original crack with a direction $\theta = \theta_0$. Therefore, we get

$$\lim_{\bar{a}\to 0^+} \bar{\sigma}_{\bar{y}} = \sigma_{\theta\theta}|_{\theta=\theta_0} \tag{4}$$

$$\lim_{\bar{a}\to 0^+} \bar{\tau}_{\bar{x}\bar{y}} = \tau_{r\theta}|_{\theta=\theta_0} \tag{5}$$

The SIFs for the branch crack, $\bar{K}_{\mathrm{I}\theta}$ and $\bar{K}_{\mathrm{II}\theta}$, can be also written as

$$\bar{K}_{\mathrm{I}\theta} = \lim_{\bar{a}\to 0^+} \sqrt{2\pi r}\,\bar{\sigma}_{\bar{y}} = \sqrt{2\pi r}\,\sigma_{\theta\theta} \tag{6}$$

$$\bar{K}_{\mathrm{II}\theta} = \lim_{\bar{a}\to 0^+} \sqrt{2\pi r}\,\bar{\tau}_{\bar{x}\bar{y}} = \sqrt{2\pi r}\,\tau_{r\theta} \tag{7}$$

Thus, when the fracture initiation takes place from the original crack in the direction $\theta = \theta_0$, the energy release rate for the branch crack, G_θ, can be obtained [21]

$$G_\theta = \frac{1}{E'}(\bar{K}_{\mathrm{I}\theta}^2 + \bar{K}_{\mathrm{II}\theta}^2) = \frac{2\pi r}{E'}(\sigma_{\theta\theta}^2 + \tau_{r\theta}^2) \tag{8}$$

where E' takes the value of E for plane stress condition and $E/(1-\nu^2)$ for plane strain condition. E and ν are the elastic modulus and Poisson's ratio, respectively. Eq. (8) indicates that the energy release rate due to the initiation of a branch crack only depends on the stress state before fracture begins. Through substituting the Eqs. (1–3) into Eq. (8) and ignoring the high order term $O(r^{1/2})$, the energy release rate G_θ can be obtained as follows,

$$G_\theta = \frac{1}{E'}[B_1 K_{\mathrm{I}}^2 + B_2 K_{\mathrm{II}}^2 + B_3 K_{\mathrm{I}} K_{\mathrm{II}} + B_4\sqrt{2\pi r}\,K_{\mathrm{I}} T + B_5\sqrt{2\pi r}\,K_{\mathrm{II}} T + B_6(2\pi r)T^2] \tag{9}$$

where

$$B_1 = \frac{1}{4}(\cos\theta+1)^2$$

$$B_2 = -3\sin^4\frac{\theta}{2} + 2\sin^2\frac{\theta}{2} + 1$$

$$B_3 = -\frac{1}{2}\sin(2\theta) - \sin\theta$$

$$B_4 = -4\cos^5\frac{\theta}{2} + 4\cos^3\frac{\theta}{2} \tag{10}$$

$$B_5 = 4\sin^5\frac{\theta}{2} - 4\sin\frac{\theta}{2}$$

$$B_6 = \sin^2\theta$$

According to the generalized G criterion, fracture takes place from the crack tip along the direction (θ_0) of maximum energy release rate. When the energy release rate along the direction θ_0 and at a critical distance r_c from the crack tip reaches its critical value, the crack initiation will take place along the fracture initiation angle θ_0. Therefore, the fracture initiation angle θ_0 can be determined by the following equations.

$$\left.\frac{\partial G_\theta}{\partial\theta}\right|_{\theta=\theta_0,\ r=r_c} = 0; \quad \left.\frac{\partial^2 G_\theta}{\partial\theta^2}\right|_{\theta=\theta_0,\ r=r_c} < 0 \tag{11}$$

Substituting the Eq. (9) into Eq. (11),

$$C_1 K_{\mathrm{I}}^2 + C_2 K_{\mathrm{II}}^2 + C_3 K_{\mathrm{I}} K_{\mathrm{II}} + C_4\sqrt{2\pi r_c}\,K_{\mathrm{I}} T + C_5\sqrt{2\pi r_c}\,K_{\mathrm{II}} T + C_6(2\pi r_c)T^2 = 0 \tag{12}$$

in which

$$C_1 = -\frac{1}{4}\sin(2\theta) - \frac{1}{2}\sin\theta$$

$$C_2 = \frac{3}{4}\sin(2\theta) - \frac{1}{2}\sin\theta$$

$$C_3 = -2\cos^2\theta - \cos\theta + 1 \tag{13}$$

$$C_4 = 10\sin^5\frac{\theta}{2} - 14\sin^3\frac{\theta}{2} + 4\sin\frac{\theta}{2}$$

$$C_5 = 10\cos^5\frac{\theta}{2} - 20\cos^3\frac{\theta}{2} + 8\cos\frac{\theta}{2}$$

$$C_6 = \sin(2\theta)$$

It is found that the fracture initiation angle θ_0 depends on the SIFs, T-stress and critical distance r_c from the crack tip. The critical distance r_c, usually correlated to the size of a damage zone around the crack tip, experiences large strains or contains a large amount of microcracks if the fracture occurs [15]. The micromechanical model of brittle fracture indicates that the crack initiates from the boundary of damage zone instead of crack tip, mainly due to the high strains near the crack tip [15,36]. Likewise, this factor is correlated to the radius of fracture process zone (FPZ) around the crack tip in brittle and quasi-brittle materials [34,36]. In practical, critical distance r_c is often considered as a constant material property that is independent of the specimen geometry and loading conditions [26,32,34]. According to the Schmidt's model [37], the critical distance r_c is given as follows,

$$r_c = \frac{1}{2\pi}\left(\frac{K_{\mathrm{Ic}}}{\sigma_t}\right)^2 \tag{14}$$

in which σ_t is the material tensile strength and K_{Ic} is the pure mode I fracture toughness of the material. The material constants σ_t and K_{Ic} can be determined experimentally by uncracked Brazilian disc (BD) specimen [33] and CCBD specimen, respectively.

When the energy release rate at crack tip reaches a critical value, the crack starts to grow. At this time,

$$G_\theta = G_{\theta c} \tag{15}$$

where $G_{\theta\mathrm{c}}$ is the critical value of the energy release rate at the critical distance r_c. Combining the Eqs. (9) and (15),

$$G_{\theta c} = \frac{1}{E'}[B_1 K_{\mathrm{I}}^2 + B_2 K_{\mathrm{II}}^2 + B_3 K_{\mathrm{I}} K_{\mathrm{II}} + B_4\sqrt{2\pi r_c}\,K_{\mathrm{I}} T + B_5\sqrt{2\pi r_c}\,K_{\mathrm{II}} T + B_6(2\pi r_c)T^2] \tag{16}$$

Both $G_{\theta\mathrm{c}}$ and r_c are assumed to be constant characteristics of the material [26,32,34].

For pure mode I fracture, $K_{\mathrm{II}} = 0$ and $\theta_0 = 0^\circ$. By replacing $K_{\mathrm{II}} = 0$ and $\theta_0 = 0^\circ$ into Eq. (16), the following equation can be obtained.

$$G_{\theta c} = \frac{1}{E'}K_{\mathrm{Ic}}^2 \tag{17}$$

Therefore, the $G_{\theta\mathrm{c}}$ can be obtained from the condition of pure mode I loading in testing. Further, the Eq. (16) can be rewritten as

$$K_{\mathrm{Ic}}^2 = B_1 K_{\mathrm{I}}^2 + B_2 K_{\mathrm{II}}^2 + B_3 K_{\mathrm{I}} K_{\mathrm{II}} + B_4\sqrt{2\pi r_c}\,K_{\mathrm{I}} T + B_5\sqrt{2\pi r_c}\,K_{\mathrm{II}} T + B_6(2\pi r_c)T^2 \tag{18}$$

The Eq. (18) can be used to predict the initiation of the mixed mode I/II crack.

3. Theoretical model

In this section, the generalized G criterion is employed to predict the initiation of the mixed mode I/II crack for three types of specimens, CCBD, SCB and ECT specimens, as shown in Fig. 3. P is a concentrated force applied to specimens, R is the radius of the CCBD and SCB specimens, W is the size of the ECT samples, and S is the half distance between the two bottom supports for SCB and ECT samples. It should be noted that a is the half-crack length for CCBD specimens and the crack length for SCD and ECT specimens. Three groups of dimensionless

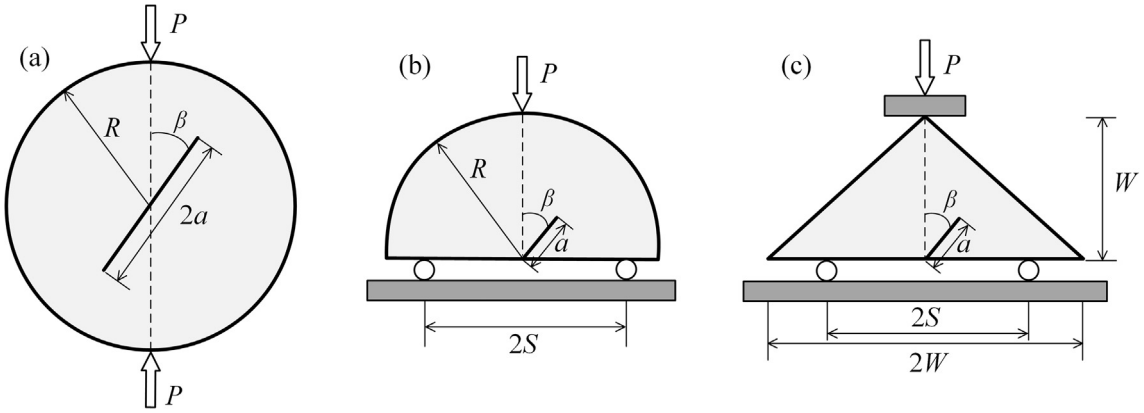

Fig. 3. Schematics of three types of specimens: (a) central cracked Brazilian disk (CCBD) specimen, (b) cracked semi-circular bend (SCB) specimen and (c) edge-crack triangular (ECT) specimen.

parameters, a/R (or a/W), S/R (or S/W), and β, are used to describe the loading conditions. a/R or a/W is the dimensionless crack length, i.e. the ratio of crack length to the sample size; S/R or S/W is the ratio of half distance between two bottom supports to sample size; β is the crack inclination angle between the applied load direction and crack direction. For a mixed mode I/II fracture, the mode mixity factor M^e is defined as [15,18]

$$M^e = \frac{2}{\pi} tan^{-1}\left(\frac{K_I}{K_{II}}\right) \tag{19}$$

where M^e varies between 0 and 1. $M^e = 1$ represents the pure mode I fracture and $M^e = 0$ represents the pure mode II fracture. M^e can be tuned by changing the crack inclination angle β. A pure mode I fracture (i.e. $M^e = 1$) is achieved by setting $\beta = 0^\circ$, while a pure mode II crack (i.e. $M^e = 0$) is achieved by setting β as a critical value, which depends on a/R for CCBD specimens, a/R and S/R for SCB specimens, and a/W and S/W for ECT specimens, respectively. For example, for the SCB specimen with $a/R = 0.3$ and $S/R = 0.43$, a pure mode II crack (i.e. $M^e = 0$) is achieved by setting $\beta = 50^\circ$.

SIFs and T-stress in the CCBD, SCB and ECT specimens can be written as follows,

$$K_i = \begin{cases} \frac{P}{RB}\sqrt{2\pi R}\, K_i^*(a/R, \beta) \text{ For BD specimens} \\ \frac{P}{RB}\sqrt{2\pi R}\, K_i^*(a/R, S/R, \beta) \text{ For SBD specimens} \\ \frac{P}{WB}\sqrt{2\pi R}\, K_i^*(a/W, S/W, \beta) \text{ For ECT specimens} \end{cases} \quad (i\text{=I, II}) \tag{20}$$

$$T = \begin{cases} \frac{4P}{RB} T^*(a/R, \beta) \text{ For BD specimens} \\ \frac{4P}{RB} T^*(a/R, S/R, \beta) \text{ For SBD specimens} \\ \frac{4P}{WB} T^*(a/W, S/W, \beta) \text{ For ECT specimens} \end{cases} \quad (i\text{=I, II}) \tag{21}$$

where B is specimen thickness. When the concentrated force P is fracture load P_f, K_i (i = I, II) will be fracture resistances K_{if} (i = I, II). K_I^*, K_{II}^* and T^* are dimensionless SIFs and T-stress that are functions of a/R (or a/W), S/R (or S/W) and β. Dimensionless SIFs (K_I^* and K_{II}^*) and T-stress (T^*) can be calculated by finite element method, over-determined method [38], interaction integral method [33,39] and so on. For example, the dimensionless parameters K_I^*, K_{II}^* and T^* in terms of crack inclination angle β are given in Fig. 4 for different types of specimens (CCBD specimen with $a/R = 0.3$, SCB specimen with $a/R = 0.3$ and $S/R = 0.43$, and ECT specimen with $a/W = 0.3$ and $S/W = 0.43$), respectively.

By substituting the Eqs. (20) and (21) into Eq. (12), we obtain

$$C_1(K_I^*)^2 + C_2(K_{II}^*)^2 + C_3 K_I^* K_{II}^* + 4C_4\sqrt{\frac{r_c}{R}} K_I^* T^* + 4C_5\sqrt{\frac{r_c}{R}} K_{II}^* T^* + 16C_6\left(\frac{r_c}{R}\right)(T^*)^2 = 0 \tag{22}$$

Therefore, the fracture initiation angle θ_0 can be obtained from the Eq. (22). It is found that the fracture initiation angle θ_0 only depends on the critical distance r_c from the crack tip, if the sample size and boundary conditions are given. Substituting the Eqs. (20) and (21) and θ_0 into Eq. (18), we obtain

$$K_{Ic}^2 = K_{If}^2\left[B_1 + B_2\left(\frac{K_{II}^*}{K_I^*}\right)^2 + B_3\frac{K_{II}^*}{K_I^*} + 4B_4\sqrt{\frac{r_c}{R}}\frac{T^*}{K_I^*} + 4B_5\sqrt{\frac{r_c}{R}}\frac{K_{II}^* T^*}{(K_I^*)^2} + 16B_6\frac{r_c}{R}\left(\frac{T^*}{K_I^*}\right)^2\right] \tag{23}$$

or

$$K_{Ic}^2 = K_{IIf}^2\left[B_1\left(\frac{K_I^*}{K_{II}^*}\right)^2 + B_2 + B_3\frac{K_I^*}{K_{II}^*} + 4B_4\sqrt{\frac{r_c}{R}}\frac{K_I^* T^*}{(K_{II}^*)^2} + 4B_5\sqrt{\frac{r_c}{R}}\frac{T^*}{K_{II}^*} + 16B_6\frac{r_c}{R}\left(\frac{T^*}{K_{II}^*}\right)^2\right] \tag{24}$$

where K_{If} and K_{IIf} are the fracture resistances with respect to the mode I and mode II cracks, respectively. Rewriting the Eqs. (23) and (24), we obtain

$$K_{If} = \frac{K_{Ic}}{\sqrt{B_1 + B_2\left(\frac{K_{II}^*}{K_I^*}\right)^2 + B_3\frac{K_{II}^*}{K_I^*} + 4B_4\sqrt{\frac{r_c}{R}}\frac{T^*}{K_I^*} + 4B_5\sqrt{\frac{r_c}{R}}\frac{K_{II}^* T^*}{(K_I^*)^2} + 16B_6\frac{r_c}{R}\left(\frac{T^*}{K_I^*}\right)^2}} \tag{25}$$

$$K_{IIf} = \frac{K_{Ic}}{\sqrt{B_1\left(\frac{K_I^*}{K_{II}^*}\right)^2 + B_2 + B_3\frac{K_I^*}{K_{II}^*} + 4B_4\sqrt{\frac{r_c}{R}}\frac{K_I^* T^*}{(K_{II}^*)^2} + 4B_5\sqrt{\frac{r_c}{R}}\frac{T^*}{K_{II}^*} + 16B_6\frac{r_c}{R}\left(\frac{T^*}{K_{II}^*}\right)^2}} \tag{26}$$

Therefore, Eqs. (22), (25) and (26) can be used to predict the initiation of the mixed mode I/II crack for the CCBD, SCB and ECT specimens. When T-stress is not considered, the generalized G criterion will be simplified to the traditional G criterion. It should be pointed out that the predictions of the traditional G criterion are the same as those of MTS criterion [21].

Eqs. (22), (25) and (26) indicate that the critical distance r_c significant affects the fracture initiation angles and fracture resistances in the generalized G criterion. Therefore, it is necessary to evaluate the

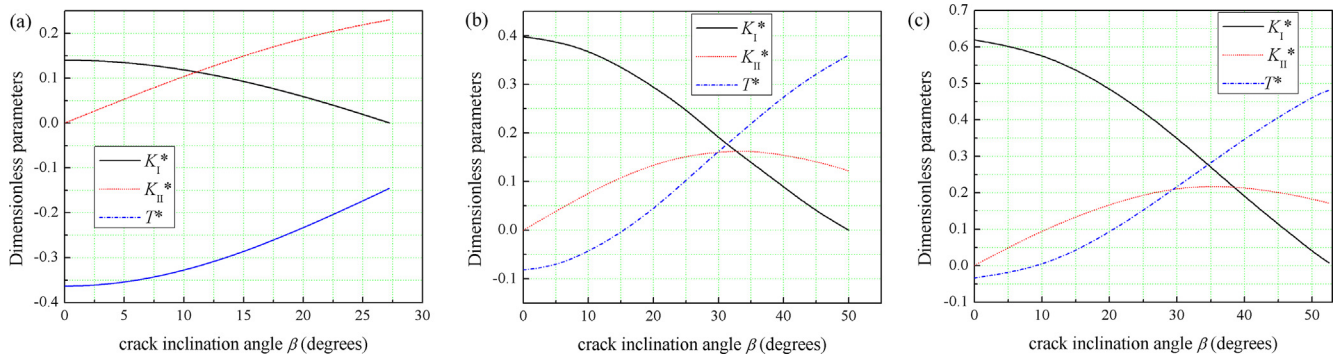

Fig. 4. The dimensionless parameters K_I^*, K_{II}^* and T^* for different types of specimens: (a) CCBD specimen with $a/R = 0.3$; (2) SCB specimen with $a/R = 0.3$ and $S/R = 0.43$; and (3) ECT specimen with $a/W = 0.3$ and $S/W = 0.43$.

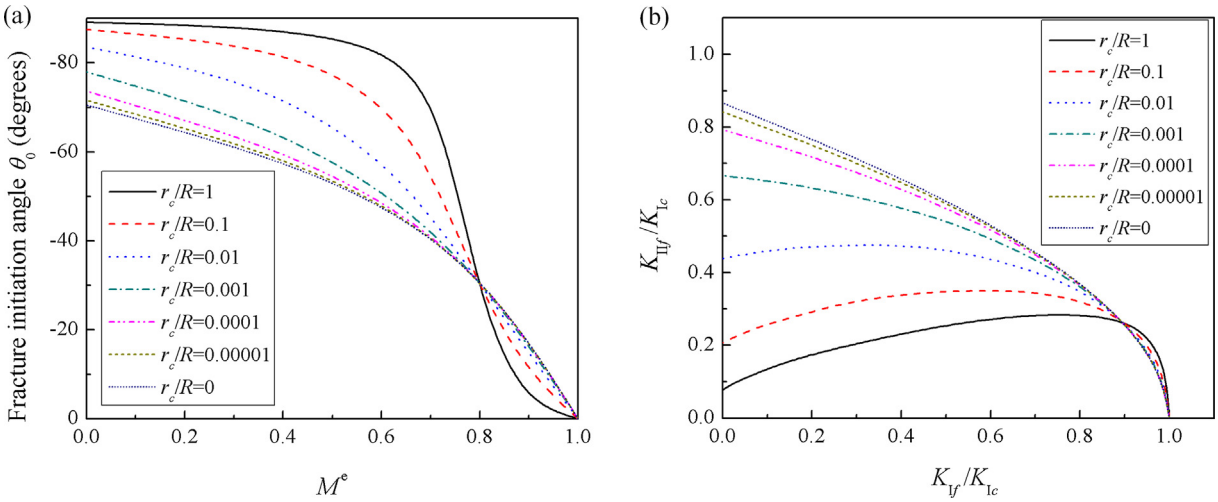

Fig. 5. The effects of r_c on theoretical prediction curves of (a) fracture initiation angles and (b) fracture resistances for SCB specimen with $a/R = 0.3$ and $S/R = 0.43$ using the generalized G criterion.

effects of r_c on fracture initiation angles and fracture resistances. Here, an example of SCB specimen with $a/R = 0.3$ and $S/R = 0.43$ is used to discuss the effects of r_c on the theoretical prediction curves of fracture initiation angles and fracture resistances, as shown in Fig. 5. The dimensionless parameters K_I^*, K_{II}^* and T^* for SCB specimen are given in Fig. 4(b). Fig. 5(a) gives the relationship of the theoretical prediction values of fracture initiation angles θ_0 in terms of mode mixity factor M^e under different values of r_c/R. It is found that the curves of fracture initiation angles significantly shift when r_c/R varies from 0 to 1. For a fixed SCB specimen with radius R, the fracture initiation angles θ_0 increase with the increasing of r_c when the mode II crack dominates. Fig. 5(b) shows the variations of the theoretical prediction curves of mixed mode I/II fracture resistances under different values of r_c/R. It is found that the theoretical prediction curves significantly depend on the values of r_c/R. For a fixed SCB specimen with radius R, the fracture resistances K_{IIf} are decreasing as r_c increases when the mode II crack dominates. Fig. 5 indicates that the effect of T-stress can be ignored and the generalized G criterion is reduced into the traditional G criterion if r_c approaches to zero. It indicates that the contribution of T-stress in the generalized G criterion can be tuned by varying the values of r_c. Once the value of r_c is determined, the contribution of T-stress in the generalized G criterion is determined accordingly. Therefore, selecting an appropriate value of r_c in the generalized G criterion is significantly important on prediction accuracy. Generally, the critical distance r_c is defined as the radius of FPZ for brittle materials with the expression of Eq. (14) [15,18].

4. Results and discussion

Experimental results from the mixed mode fracture tests on CCBD specimens are first used to examine the validation of generalized G criterion [26,33,34]. A series of experiments are conducted using Harsin marble by Aliha and Ayatollahi [34]. The CCBD samples are designed as the rock cylinders with a diameter of 110 mm and a thickness of 25 mm. A hole with a diameter of 2 mm is drilled in the center disc and a center crack is created by a thin fret saw blade of 0.5 mm thickness. The length of center crack $2a$ is chosen as 33 mm and the ratio of a/R is 0.3. The crack inclination angles β are set as 0° (pure mode I), 4°, 8°, 12°, 16°, 20°, 24° and 27° (pure mode II). A series of compression tests are conducted to measure the fracture initiation angles θ_0 and the fracture resistances K_{If} and K_{IIf}. To determine the critical distance r_c, tensile strength σ_t and fracture toughness K_{Ic} are measured as 7.2 MPa and 1 MPa·m$^{1/2}$ from a series of BD and CCBD tests [15,18]. Thus, r_c for the Harsin marble is calculated as 3.07 mm, according to Eq. (14). More information about these experiments can be found in the literature [34]. The dimensionless SIFs and T-stress for CCBD specimens with $a/R = 0.3$ are given as Fig. 4(a).

Fig. 6(a) plots the fracture initiation angles in terms of the M^e theoretically calculated by generalized G and traditional G criteria, as well as experimentally obtained from the CCBD specimens. The corresponding fracture resistances of the CCBD specimens are plotted in Fig. 6(b). A significant deviation can be found between the experimental results and the theoretical predications from the traditional G criterion. In specific, the traditional G criterion overestimates fracture initiation angles while underestimates the fracture resistances for CCBD

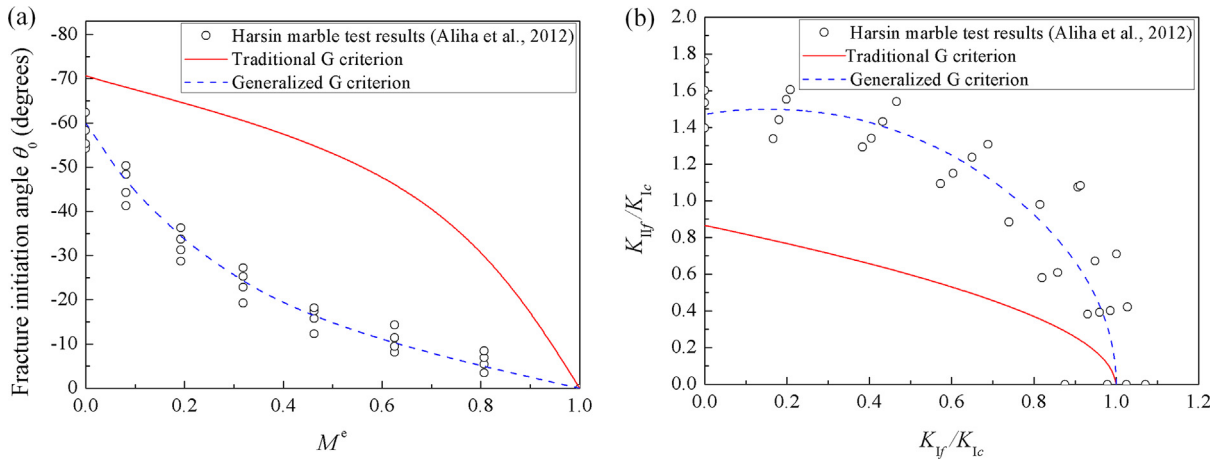

Fig. 6. Comparisons of the theoretical results calculated from generalized G and traditional G criteria versus experimental results for the CCBD specimens made of Harsin marble. (a) Fracture initiation angles and (b) fracture resistances. Data point is extracted from the experiments by Aliha and Ayatollahi [34].

specimens. However, theoretical predications from the generalized G criterion excellently fit with the experimental results, including both fracture initiation angles and the fracture resistances.

Experimental results from the mixed mode fracture test on SCB specimens are also used to validate the accuracy of the theoretical prediction from generalized G criterion [26,34]. The diameter and thicknesses of SCB specimens are the same as the CCBD specimens mentioned above. The precast crack is cut with a thin fret saw blade (0.5 mm in thickness) from the middle of the bottom edge of SCB samples. The length of center crack a, ratio of a/R and loading span ratio S/R are chosen as 16.5 mm, 0.3 and 0.43, respectively. The crack inclination angles β is designed as 0° (mode I), 10°, 20°, 30°, 40°, 43°, 47° and 50° (mode II). The r_c for Harsin marble is calculated as 3.07 mm, due to the identical material Harsin marble mentioned above. A series of 3-point bending tests are conducted to obtain the fracture initiation angles θ_0, the fracture resistances K_{If} and K_{IIf}. The dimensionless SIFs and T-stress for SCB specimens with $a/R = 0.3$ and $S/R = 0.43$ are given as Fig. 4(b).

Fig. 7(a) plots the fracture initiation angles in terms of the M^e theoretically calculated by generalized G and traditional G criteria, as well as experimentally obtained from the SCB specimens. The corresponding fracture resistances of the SCB specimens are plotted in Fig. 7(b). Similarly, the traditional G criterion fails to obtain the results that can fit well with the experimental results from fracture tests on the SCB specimens. The discrepancy between the theoretical prediction from traditional G criterion and experimental results is obvious for mode II dominated fracture. The traditional G criterion underestimates fracture initiation angles and overestimates the fracture resistances for SCB specimens, especially when the mode II crack dominates the fracture. As expected, the generalized G criterion (dash) provides a better prediction of the mixed mode fracture. It proves that the T-stress, considered within generalized G criterion, make a significant contribution on the mixed mode fracture of brittle materials.

A different material PMMA has been tested in the full range from pure mode I to pure mode II using the SCB specimens containing an edge crack by Ayatollahi et al. [26]. Similarly, the following geometry parameters of the SCB specimens $R = 50$ mm, $a = 15$ mm, $B = 5$ mm, $a/R = 0.3$ and $S/R = 0.43$ are chosen in this test. The crack inclination angles β are set as 0° (pure mode I), 10°, 20°, 30°, 40°, 43°, 47° and 50° (pure mode II). Moreover, the value of r_c of PMMA is chosen as 0.065 mm, which is the same as the literature [15,26]. Then, a series of 3-point bending tests are conducted to obtain the fracture resistances K_{If} and K_{IIf}. Likewise, the prediction curves of the generalized G criterion as well as traditional G criterion for fracture resistances of the SCB specimens made of PMMA are shown in Fig. 8. It is found that the generalized G criterion can more accurately predict the mixed mode fracture behavior of PMMA than the traditional G criterion.

Experimental results [27] from the mixed mode fracture tests on ECT specimens in Neiriz marble also confirm the high accuracy of the theoretical prediction from generalized G criteria. In the experiments, ECT specimen (Fig. 3(c)) is designed as a right-angled triangular plate with base length $2W = 150$ mm, and located inside the three-point

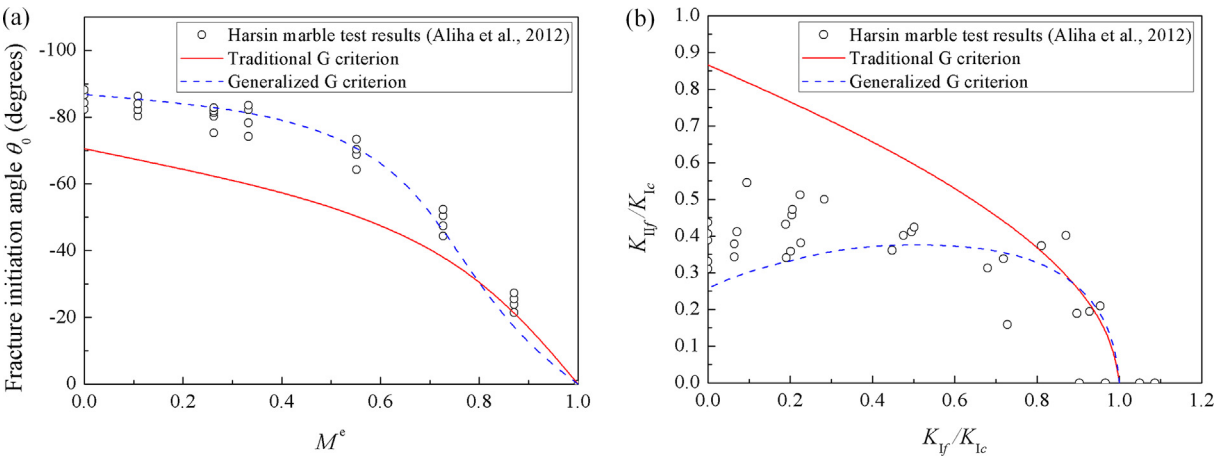

Fig. 7. Comparisons of the theoretical results calculated from generalized G and traditional G criteria versus the experimental results for the SCB specimens made of Harsin marble. (a) Fracture initiation angles and (b) fracture resistances. Data points are extracted from the experiments by Aliha and Ayatollahi [34].

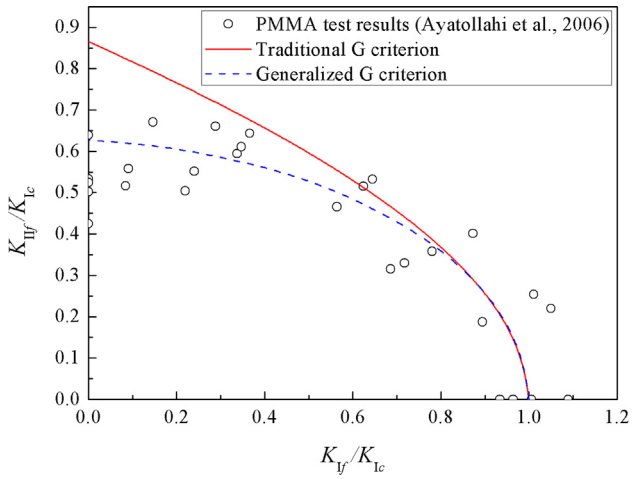

Fig. 8. Fracture resistances for the SCB specimens made of PMMA. Dash line is calculated from generalized G criterion and Solid line is calculated traditional G criterion. Data points are extracted from the experiments by Ayatollahi et al. [26].

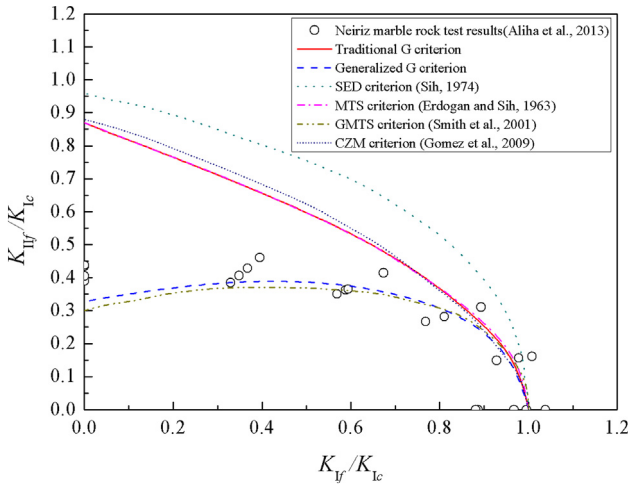

Fig. 10. Comparisons of the theoretical predictions from traditional G, generalized G, SED, MTS, GMTS and CZM criteria versus the experimental results of fracture resistances for the ECT specimens made of Neiriz marble [27].

bend fixture with the thickness $B = 16$ mm. A thin fret saw is used to prepare an initial narrow notch with the width of 0.3 mm and length of 22.5 mm. The a/W and S/W are chosen as 0.3 and 0.43, respectively. The crack inclination angles β are set as 0° (mode I), 10°, 20°, 30°, 40° and 52.5° (mode II). The fracture toughness K_{Ic} of the Neiriz marble is measured as 0.74 MPa·m$^{1/2}$ by a series of tests of CCBD samples, and the tensile strength σ_t is 5.64 MPa tested by uncracked BD samples. Therefore, r_c can be determined by Eq. (14) as 2.74 mm. Then, fracture initiation angles θ_0 and fracture resistances K_{If} and K_{IIf} can be obtained by a series of 3-point bending tests. The dimensionless SIFs and T-stress for ECT specimens with $a/W = 0.3$ and $S/W = 0.43$ are given as Fig. 4(c).

For ECT specimens, similar conclusions with those in Figs. 6 and 7 can be found in Fig. 9. The traditional G criterion fails to offer good predictions for the experimental results from the ECT specimens. The traditional G criterion underestimates fracture initiation angles and overestimates the fracture resistances for ECT specimens, especially when the mode II crack dominates the fracture. The generalized G criterion provides better predictions of the mixed mode fracture for the ECT specimens, including the fracture initiation angles and fracture resistances, as shown in Fig. 9. Further, the theoretical predictions of fracture resistances obtained from traditional G, generalized G, SED, MTS, GMTS and CZM criteria on the ECT specimens are compared in Fig. 10 [27]. It is found that the results predicted by traditional G, SED, MTS and CZM criteria are not in agreement with the experimental results, due to the neglection of the influence from T-stress. However, with considering the influence from T-stress, such as the theoretical predictions from the generalized G criterion and GMTS criterion, an excellent agreement with the experimental results can be found.

5. Conclusions

In this work, a modified energy-based criterion (generalized G criterion) is proposed to study the mixed mode I/II fracture behaviors for brittle and quasi-brittle materials. The generalized G criterion includes both the singular stress terms (SIFs) and the first non-singular term (T-stress) in Williams' series expansion on the calculation of energy release rate. The experimental results from the mixed mode fracture analysis of the materials, PMMA, Harsin marble and Neiriz marble, using CCBD, SCB and ECT specimens are used to validate the generalized G criterion. The theoretical prediction of the fracture initiation angles and crack onset from the generalized G criterion are compared with that from traditional G criterion. The following conclusions can be achieved:

(1) The traditional G criterion only including the singular stress terms overestimates or underestimates the fracture initiation angles and fracture resistances, especially when the mode II crack dominates

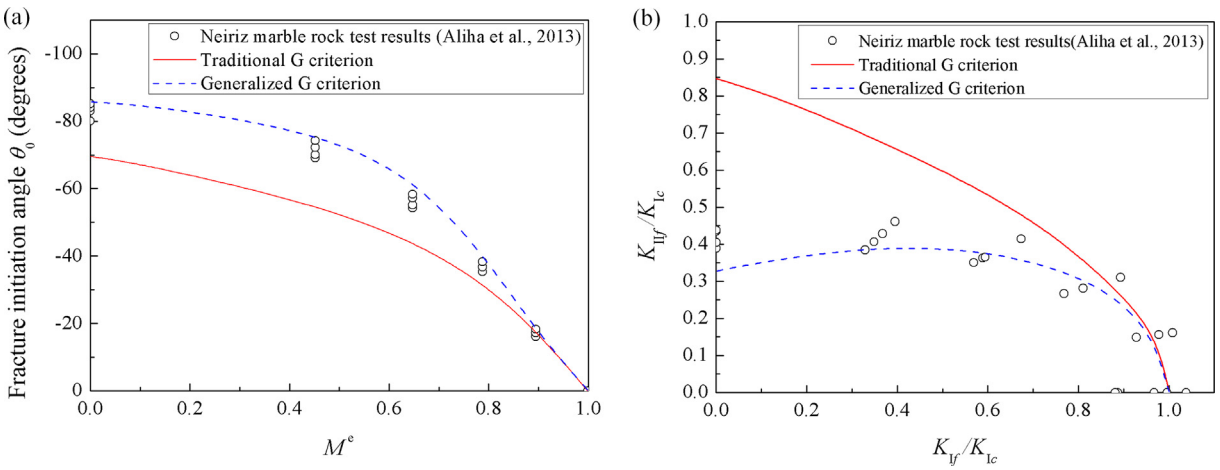

Fig. 9. Comparisons of the theoretical results calculated from generalized G and traditional G criteria versus the experimental results for the ECT specimens made of Neiriz marble. (a) Fracture initiation angles and (b) fracture resistances. Data points are extracted from the experiments by Aliha et al. [27].

the fracture.

(2) The theoretical predictions of fracture initiation angles and fracture resistances from the generalized G criterion are in great agreement with the experimental results.

(3) T-stress plays an important role on the fracture analysis of the materials under mixed mode loading.

Acknowledgements

This work was supported by National Natural Science Foundation of China (Grant Nos. 1171101165, 11602188, 11702186 and 11472204) and National Defense Key Laboratory Fund of China (Grant No. 614220207011017).

References

[1] T.J. Wang, A continuum damage model for ductile fracture of weld heat affected zone, Eng. Fract. Mech. 40 (6) (1991) 1075–1082.
[2] T.J. Wang, Z. Lou, A continuum damage model for weld heat affected zone under low cycle fatigue loading, Eng. Fract. Mech. 37 (4) (1990) 825–829.
[3] T.J. Wang, Improvements of J-integral criterion for ductile fracture characterized by a triaxiality parameter, Eng. Fract. Mech. 48 (2) (1994) 207–216.
[4] F.J. Gómez, M. Elices, F. Berto, P. Lazzarin, Fracture of U-notched specimens under mixed mode: experimental results and numerical predictions, Eng. Fract. Mech. 76 (2) (2009) 236–249.
[5] L. Marsavina, D.M. Constantinescu, E. Linul, D.A. Apostol, T. Voiconi, T. Sadowski, Refinements on fracture toughness of PUR foams, Eng. Fract. Mech. 129 (2014) 54–66.
[6] R. Negru, L. Marsavina, T. Voiconi, E. Linul, H. Filipescu, G. Belgiu, Application of TCD for brittle fracture of notched PUR materials, Theor. Appl. Fract. Mech. 80 (2015) 87–95.
[7] F. Erdogan, G.C. Sih, On the crack extension in plates under plane loading and transverse shear, J. Basic Eng. ASME 85 (1963) 519–525.
[8] D.J. Smith, M.R. Ayatollahi, M.J. Pavier, The role of T-stress in brittle fracture for linear elastic materials under mixed-mode loading, Fatigue Fract. Eng. M. 24 (2) (2001) 137–150.
[9] J. Akbardoost, M.R. Ayatollahi, Experimental analysis of mixed mode crack propagation in brittle rocks: the effect of non-singular terms, Eng. Fract. Mech. 129 (2014) 77–89.
[10] K.J. Chang, On the maximum strain criterion—a new approach to the angled crack problem, Eng. Fract. Mech. 14 (1) (1981) 107–124.
[11] M.M. Mirsayar, Mixed mode fracture analysis using extended maximum tangential strain criterion, Mater. Design 86 (2015) 941–947.
[12] M.M. Mirsayar, A. Razmi, M.R.M. Aliha, F. Berto, EMTSN criterion for evaluating mixed mode I/II crack propagation in rock materials, Eng. Fract. Mech. 190 (2018) 186–197.
[13] W. Hua, S. Dong, X. Pan, Q. Wang, Mixed mode fracture analysis of CCBD specimens based on the extended maximum tangential strain criterion, Fatigue Fract. Eng. M. 40 (2017) 2118–2127.
[14] G.C. Sih, Strain-energy-density factor applied to mixed mode crack problems, Int. J. Fract. 10 (3) (1974) 305–321.
[15] M.R. Ayatollahi, M.R. Moghaddam, F. Berto, A generalized strain energy density criterion for mixed mode fracture analysis in brittle and quasi-brittle materials, Theor. Appl. Fract. Mech. 79 (2015) 70–76.
[16] P. Lazzarin, R. Zambardi, A finite-volume-energy based approach to predict the static and fatigue behavior of components with sharp V-shaped notches, Int. J. Fract. 112 (3) (2001) 275–298.
[17] L. Marsavina, F. Berto, R. Negru, D.A. Serban, E. Linul, An engineering approach to predict mixed mode fracture of PUR foams based on ASED and micromechanical modelling, Theor. Appl. Fract. Mech. 91 (2017) 148–154.
[18] M.R. Moghaddam, M.R. Ayatollahi, F. Berto, Mixed mode fracture analysis using generalized averaged strain energy density criterion for linear elastic materials, Int. J. Solids Struct. 120 (2017) 137–145.
[19] K. Palaniswamy, Crack Propagation Under General In-Plane Loading, Ph.D. Thesis, California Institute of Technology, 1972.
[20] M.A. Hussain, S.L. Pu, J. Underwood, Strain Energy Release Rate for a Crack Under Combined Mode I and Mode II, Fracture Analysis, ASTM STP 560, American Society for Testing and Materials, Philadelphia, 1974.
[21] R.J. Nuismer, An energy release rate criterion for mixed mode fracture, Int. J. Fract. 11 (2) (1975) 245–250.
[22] C.H. Wu, Fracture under combined loads by maximum-energy-release-rate criterion, J. Appl. Mech. 45 (3) (1978) 538–553.
[23] B. Li, X.L. Fan, H. Okada, T.J. Wang, Mechanisms governing the failure modes of dense vertically cracked thermal barrier coatings, Eng. Fract. Mech. 189 (2018) 451–480.
[24] M.R.M. Aliha, M.R. Ayatollahi, Analysis of fracture initiation angle in some cracked ceramics using the generalized maximum tangential stress criterion, Int. J. Solids Struct. 49 (13) (2012) 1877–1883.
[25] M.R.M. Aliha, M.R. Ayatollahi, D.J. Smith, M.J. Pavier, Geometry and size effects on fracture trajectory in a limestone rock under mixed mode loading, Eng. Fract. Mech. 77 (11) (2010) 2200–2212.
[26] M.R. Ayatollahi, M.R.M. Aliha, M.M. Hassani, Mixed mode brittle fracture in PMMA—an experimental study using SCB specimens, Mater. Sci. Eng. A 417 (1) (2006) 348–356.
[27] M.R.M. Aliha, G.R. Hosseinpour, M.R. Ayatollahi, Application of cracked triangular specimen subjected to three-point bending for investigating fracture behavior of rock materials, Rock Mech. Rock Eng. 46 (5) (2013) 1023–1034.
[28] W. Hua, S.M. Dong, Y. Fan, X. Pan, Q.Y. Wang, Investigation on the correlation of mode II fracture toughness of sandstone with tensile strength, Eng. Fract. Mech. 184 (2017) 249–258.
[29] Z.Z. Du, J.W. Hancock, The effect of non-singular stress on crack-tip constraint, J. Mech. Phys. Solids 39 (4) (1991) 555–567.
[30] M.R.M. Aliha, M.R. Ayatollahi, Mixed mode I/II brittle fracture evaluation of marble using SCB specimen, Proc. Eng. 10 (1) (2011) 311–318.
[31] M.R. Ayatollahi, M.R.M. Aliha, On determination of mode II fracture toughness using semi-circular bend specimen, Int. J. Solids Struct. 43 (17) (2006) 5217–5227.
[32] M.R. Ayatollahi, M.R.M. Aliha, Mixed mode fracture in soda lime glass analyzed by using the generalized MTS criterion, Int. J. Solids Struct. 46 (2) (2009) 311–321.
[33] C. Hou, Z.Y. Wang, W.G. Liang, J.B. Li, Z.H. Wang, Determination of fracture parameters in center cracked circular discs of concrete under diametral loading: a numerical analysis and experimental results, Theor. Appl. Fract. Mech. 85 (2016) 355–366.
[34] M.R.M. Aliha, M.R. Ayatollahi, J. Akbardoost, Typical upper bound-lower bound mixed mode fracture resistance envelopes for rock material, Rock Mech. Rock Eng. 45 (1) (2012) 65–74.
[35] M.L. Williams, On the stress distribution at the base of a stationary crack, J. Appl. Mech. 24 (1956) 109–114.
[36] M. Ghamgosar, N. Erarslan, Experimental and numerical studies on development of fracture process zone (FPZ) in rocks under cyclic and static loadings, Rock Mech. Rock Eng. 49 (3) (2016) 893–908.
[37] R.A. Schmidt, A microcrack model and its significance to hydraulic fracturing and fracture toughness testing, The 21st US Symposium on Rock Mechanics (USRMS), American Rock Mechanics Association, 1980.
[38] M.R. Ayatollahi, M. Nejati, An over-deterministic method for calculation of coefficients of crack tip asymptotic field from finite element analysis, Fatigue Fract. Eng. Mater. Struct. 34 (3) (2011) 159–176.
[39] C. Hou, Z.Y. Wang, W.G. Liang, H.J. Yu, Z.H. Wang, Investigation of the effects of confining pressure on SIFs and T-stress for CCBD specimens using the XFEM and the interaction integral method, Eng. Fract. Mech. 178 (2017) 279–300.